JOURNAL OF CATALYSIS 70, 14–23 (1981)

Mechanism of Methanol Oxidation over Oxide Catalysts Containing MoO_3

MIKI NIWA, MAKOTO MIZUTANI, MAMORU TAKAHASHI, AND YUICHI MURAKAMI

Department of Synthetic Chemistry, Faculty of Engineering, Nagoya University, Furo-cho, Chikusa-ku, Nagoya 464 Japan

Received April 25, 1979; revised July 23, 1980

The mechanism of methanol oxidation over a SnO_2–MoO_3 catalyst was investigated from the viewpoint of the active molybdenum site available. The Mo^{5+} on the SnO_2–MoO_3 catalyst was stabilized as a relatively unoxidizable species. The reactivity of the Mo^{5+} was determined by ESR, ir and gravimetry to be much greater than that of the Mo^{6+} for methanol oxidation over this catalyst. *In situ* measurement of the Mo^{5+} ESR signal during methanol oxidation indicates that oxidation occurs primarily at Mo^{5+} sites. A mechanism for methanol oxidation involving the oxidation-reduction cycle $Mo^{5+} \rightleftharpoons Mo^{4+}$ is proposed. The mechanism may also be valid for ethanol and 2-propanol oxidations over TiO_2–MoO_3 and MoO_3–SiO_2 catalysts.

INTRODUCTION

Since 1931 when Adkins and Peterson (*1*) discovered the high activity of the mixed Fe_2O_3–MoO_3 catalyst for oxidation of methanol to formaldehyde, most patents and fundamental research papers dealing with this process have been concerned with the Fe_2O_3–MoO_3 system. The activity may be substantially ascribed to MoO_3 which achieves enhanced activity on admixture of Fe_2O_3. Detailed studies have investigated the role of oxide composition (*2–4*) and the nature of the active sites as well as the reaction mechanism involved in methanol oxidation (*5–8*).

The authors have already examined the activities of various mixed oxides, including Fe_2O_3–MoO_3, and found higher activities over SnO_2–MoO_3 and TiO_2–MoO_3 catalysts than over Fe_2O_3–MoO_3 catalyst (*9*). In particular, the activity of the SnO_2–MoO_3 system for methanol oxidation has been investigated in detail. Methanol is selectively oxidized to formaldehyde over MoO_3 at temperatures above 350°C, but it is oxidized to carbon oxides only on SnO_2. For the mixed SnO_2–MoO_3 catalysts, however, formaldehyde was formed selectively even at 180°C. These activities were nearly independent of the catalyst composition in the range of Sn : Mo ratios from 1 : 9 to 7 : 3. Furthermore, in a freshly oxidized state, these catalysts exhibited an ESR signal due to paramagnetic Mo^{5+}. The relative concentration of Mo^{5+} in these catalysts as determined by ESR spectroscopy at 77 K appeared to be correlated with the catalytic activity. In the present communication, the activity of the SnO_2–MoO_3 catalyst, especially as it relates to the role of the Mo^{5+}, is investigated in detail.

It has been reported that in a variety of cases the catalytic activity may be correlated with the signal intensity of the Mo^{5+} (*10–15*). However, the catalytic activity of Mo^{5+} is not fully understood, and it has not been confirmed that the Mo^{5+} sites are actually available for the reaction. Provided that an ESR signal can be detected at reaction temperatures without interference from other signals, the behavior of the paramagnetic metal ion may be observed under reaction conditions. Sancier *et al.* (*13*) have previously utilized this method of using a "Reactor Cell" to investigate the mechanism of propylene oxidation over

0021-9517/81/070014-10$02.00/0

Bi_2O_3–MoO_3/SiO_2. In the study presented here, the Mo^{5+} signals from SnO_2–MoO_3, TiO_2–MoO_3, and MoO_3–SiO_2 were examined in conjunction with kinetic measurements to elucidate the mechanism of methanol oxidation over these catalysts.

EXPERIMENTAL

Catalyst. The SnO_2–MoO_3 catalyst was prepared by mixing of tin(IV) hydroxide gel with ammonium molybdate solution, drying in a 120°C oven, and then calcining at 500°C for 3 hr in an air stream. The $Sn(OH)_4$ gel used was precipitated by the addition of $SnCl_4 \cdot 2H_2O$ to aqueous ammonia solution and then washed with water to remove Cl^- ion. The TiO_2–MoO_3 catalyst was obtained by mixing an ammonium molybdate solution with tetraethyl orthosilicate in a vibration mixer enclosed in a water bath. The resulting gel was thoroughly mixed in a kneader.

ESR. ESR measurements were performed in the X-band with a JEOL spectrometer (JES-ME-1X). The ESR *in situ* cell was made of a 3 mm i.d. Pyrex outer tube and a 1 mm o.d. inner tube which was set in a cavity equipped with a variable temperature attachment. CH_3OH, O_2, and N_2 were passed into the ESR *in situ* cell under the same conditions of reaction temperature, catalyst weight, total flow rate, and partial pressures as the normal continuous-flow reaction. The ESR spectra of the oxides were measured during the oxidation reactions. The radical concentration was determined by comparison with a KBr diluted coke sample, and g values were determined by comparison with Mn^{2+} impurity in MgO.

ir. Infrared spectra of untreated or treated SnO_2–MoO_3 samples were recorded on an emissionless diffuse reflectance spectrophotometer (JASCO IRA-3S) (*16*) at room temperature. ir samples were 3.0 wt% catalyst/KBr mixtures.

Gravimetry. Weight loss from SnO_2–MoO_3 by reduction or oxidation was measured gravimetrically using a quartz spring microbalance with a constant of 207 mg/cm in a doubly sealed vessel. CCl_4 vapor was admitted to the outer tube to keep a constant temperature. Expansion of the balance was monitored with a cathetometer.

Kinetics. Catalyst (0.2 g) was placed in a reactor made of 10 mm i.d. Pyrex glass and heated in a sand bath. A gas mixture of O_2, N_2, and CH_3OH was passed into the reactor at a total flow rate of 70 ml/min, and the products were injected into a gas chromatograph through a gas-sampling valve. The gas chromatograph was constructed of two TCD detectors. A sucrose octaacetate on Daiflon column at 80°C was used for separation of the CH_3OH and HCHO components of the mixture. These components were analyzed prior to passage of the mixture through a 0.5 m Porapak T column at room temperature which allowed analysis for CO_2 after returning the gases through the opposite side of the first detector. O_2, N_2, and CO were then separated from the mixture by a 2 m Molecular Sieve 13X column at room temperature and analyzed in the second detector.

RESULTS

Behavior of Mo^{5+} on SnO_2–MoO_3

As mentioned previously, the activity of different SnO_2–MoO_3 catalyst is nearly independent of the Sn/Mo ratio. The 3:7 SnO_2–MoO_3 is used as an example in a following description.

Figure 1 shows an anisotropic ESR signal formed at $g = 1.92$ for SnO_2–MoO_3 in the *in situ* reactor at 180°C. This signal can be

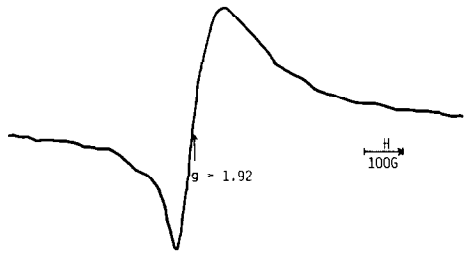

FIG. 1. ESR spectrum of Mo^{5+} on SnO_2–MoO_3 under reaction conditions.

observed also for pure MoO_3, but not for SnO_2. By comparison with the data in the literature (*10–15*), the signal can be assigned to the paramagnetic Mo^{5+}. The linewidth of this signal is close to that observed under vacuum, and it is not influenced by the presence of oxygen or methanol.

Sancier *et al.* (*18*) has proposed that the surface Mo^{5+} on Bi_2O_3–MoO_3 can be distinguished from the Mo^{5+} in the bulk sample by observing the decrease in signal intensity due to dipole interaction between adsorbed oxygen and paramagnetic Mo^{5+} at the surface. The influence of adsorbed oxygen on the signal intensity for the SnO_2–MoO_3 catalyst was examined at room temperature. The correlation of signal intensity with the partial pressure of oxygen on untreated and treated SnO_2–MoO_3 is shown in Fig. 2. Another unidentified signal at $g = 2.0$ was observed for the catalysts which had been either evacuated at 430°C or treated with methanol and oxygen at 200°C. Although the $g = 2.0$ signal decreased in intensity on introduction of oxygen and could be restored to the original intensity upon evacuation, the Mo^{5+} signal intensity remained virtually unchanged by this treatment. Therefore, the Mo^{5+} does not appear to interact with adsorbed oxygen at the surface and so must be highly stabilized at room temperature because it is unlikely that all of the Mo^{5+} are immersed in the bulk of the catalyst. The behavior of the Mo^{5+} on SnO_2–MoO_3 is quite different from Bi_2O_3–MoO_3 (*18*) in this respect.

The variation in Mo^{5+} signal intensity

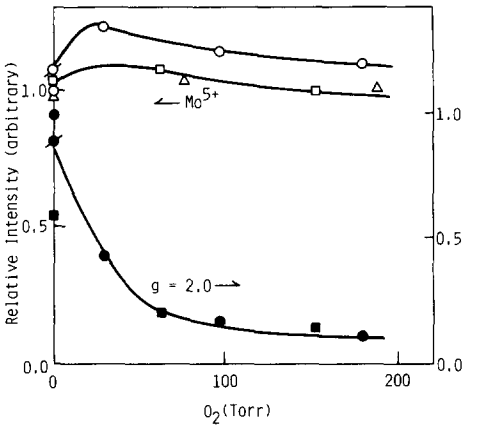

FIG. 2. Influence of partial pressure of oxygen on Mo^{5+} signal intensity at room temperature over SnO_2–MoO_3 catalyst, untreated (△), evacuated at 430°C (○, ●), and treated with methanol and oxygen at 200°C (□, ■). (⌀, ⌀); reproduced by the reevacuation of gas phase.

was then measured at 185°C in the *in situ* cell. Following oxidation, the catalyst was reduced by the addition of methanol vapor and the signal intensity was monitored as a function of time. As shown in Fig. 3, the signal intensity was recovered by oxidation of the catalyst. The rate of reoxidation was a little slower than that of reduction. The reduction–reoxidation cycle indicates that the Mo^{5+} signal exhibits its greatest intensity at the highest oxidation level of the catalyst.

Throughout these measurements no signal due to carbon deposition was observed, and since the signal width was nearly constant, about 110 G, the relative intensity of the Mo^{5+} signal was expressed in terms of

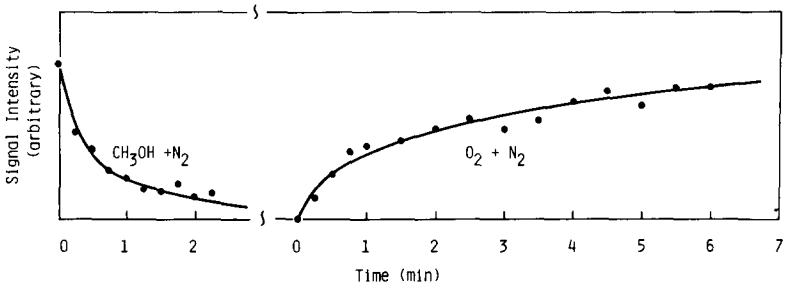

FIG. 3. The variation of signal intensity with time in methanol or oxygen flow at 185°C.

peak-to-peak height. If methanol reduced the Mo^{6+} to Mo^{5+} on the surface, the Mo^{5+} signal intensity should have increased during the reduction by methanol. It was therefore assumed that the Mo^{5+} site was reduced, but the Mo^{6+} was not reduced to Mo^{5+}.

Assuming first order kinetics for the concentrations of oxidized site and methanol, the reduction rate shown in Fig. 3 was analyzed quantitatively. The decrease of active sites by the reduction is described as

$$\log \frac{\theta_t}{\theta_0} = -\frac{k_1' P_m}{2.303} t \qquad (1)$$

where θ_t and θ_0 denote the concentrations of oxidized sites at time t and at the initial state, respectively, and P_m shows the partial pressure of methanol. k_1' is the rate constant per oxidized site for the reduction step, and is related to k_1, the rate constant per g-catalyst, as

$$k_1 = k_1' N_t, \qquad (2)$$

where N_t shows the total number of oxidized sites, i.e., 3.0×10^{18}/g-catal., the greatest value in an oxygen stream. Similar kinetic equations may be applied to the reoxidation step, but the rate of reoxidation is assumed to be proportional to the root of the partial pressure of oxygen. Plots of Eq. (1) gave straight lines from which rate constants could be calculated. Rate constants for the reduction and reoxidation of the Mo^{5+} are shown in Table 1. These values are to be compared with parameters obtained by other methods.

X-Ray diffraction patterns of fresh and aged samples of SnO_2–MoO_3 were indicative of only SnO_2 and MoO_3 and did not exhibit patterns for any new compounds. This result agrees with those obtained by Buiten (*19*) and Araki *et al.* (*20*). The crystal size of MoO_3 was calculated from the line width to be about 560 Å. Assuming that the sample contains the typical MoO_3 unit cell, about 2% of Mo atom should exist at the surface. It was estimated that roughly 5% of the surface Mo atoms could be detected as Mo^{5+} sites. In other words, most of the molybdenum oxide exists in the MoO_3 form and only a small concentration of Mo^{5+} is observed at the surface.

Infrared and Gravimetric Measurements

In order to determine the reactivity of the Mo^{6+} which is undetectable by ESR, infrared and gravimetric measurements were performed. Figure 4a shows the ir spectrum of untreated SnO_2–MoO_3 below 1100 cm^{-1}. Absorptions were observed at 985 and 880 cm^{-1}, which were attributed to Mo^{6+}=O and Mo^{6+}–O–Mo^{6+}, respectively. This is in good agreement with the report by Araki *et al.* (*20*). When the catalyst was then reduced by a methanol and nitrogen mixture in a flow reactor for 1 hr at 206°C, the intensity of absorption decreased only a little. According to Lambert–Beer's law, the Mo^{6+}=O and Mo^{6+}–O–Mo^{6+} bands decreased by 33.4 and 19.0%, respectively. These bands disappeared on reduction with methanol at 461°C. Obviously, the reduction of Mo^{6+} was much

TABLE 1

Comparison between Rate Constants Obtained from Various Experimental Methods

Experiment	Temperature (°C)	k_1 (mmol g^{-1} min^{-1} atm^{-1}) k_1' (sec^{-1} atm^{-1})	k_2 (mmol g^{-1} min^{-1} $atm^{-1/2}$) k_2' (sec^{-1} $atm^{-1/2}$)
Reduction–reoxidation Cycle by ESR	185	k_1: 1.7×10^{-1} k_1': 5.8×10^{-1}	k_2: 8.9×10^{-3} k_2': 2.9×10^{-2}
Gravimetry	203	k_1: 2.8×10^{-5}	—
Kinetics	185	k_1: 1.7×10^{0}	k_2: 1.2×10^{-1}

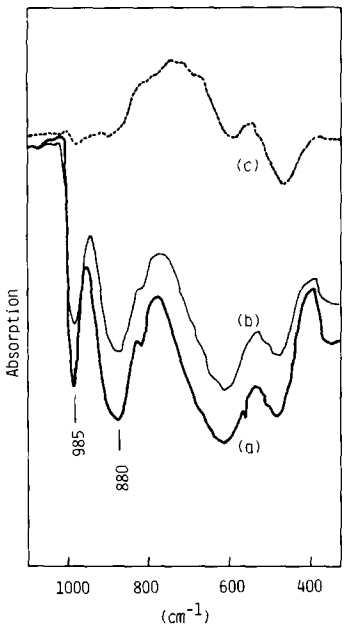

FIG. 4. Infrared spectra of the SnO_2–MoO_3 catalyst, untreated (a) and reduced by methanol at 206°C (b) and 461°C (c) for 1 hr.

slower than that of Mo^{5+}, because the latter disappeared in only 5 min at 185°C, as described above.

Weight loss during the reduction was then measured gravimetrically at 203°C. After the catalyst was fully oxidized in the vacuum-vessel, methanol vapor was introduced to reduce the catalyst at 203°C. The catalyst weight decreased gradually on reduction, as shown in Fig. 5. It reached a steady state after about 2 hr. The catalyst weight further decreased on evacuation of the gas phase, and reached a 2 wt% decrease in the most reduced condition. Finally, reoxidation by oxygen increased the catalyst weight, but did not recover its initial state.

If the catalyst is fully reduced, i.e., SnO_2 and MoO_3 become SnO and MoO_2, the catalyst weight should decrease by 11 wt%. However, only a 2 wt% decrease was observed under these conditions. Consequently, a reduction for 2 hr at 203°C results in incomplete reduction. As with the infrared study, the reduction of the entire catalyst by methanol is very slow compared to the Mo^{5+} reduction.

If the increase in weight due to adsorption of methanol is neglected, the rate constant for the reduction may be calculated based on Eq. (1). As clearly shown in Table 1, the rate constant, k_1, derived from gravimetric measurement is much smaller than that for the reduction of Mo^{5+} determined by ESR measurement. It is considered that the few assumptions necessary for deriving k_1 from Fig. 5 have only a small influence on this result. Therefore, the Mo^{5+} can be regarded as a highly reactive oxidized site in comparison to the Mo^{6+}.

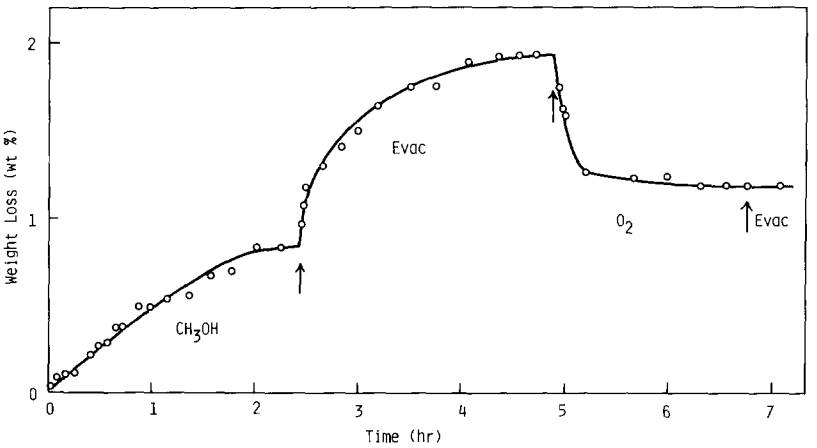

FIG. 5. Time dependence of weight loss over SnO_2–MoO_3.

Kinetics and in Situ Measurements on SnO_2–MoO_3

The mechanism of methanol oxidation has been previously analyzed by several investigators. The ideas regarding the oxidation–reduction mechanism proposed by Jiru *et al.* (*5*) were experimentally confirmed, and consistently followed in concurrent studies by Mann and Hahn (*21*) and Pernicone *et al.* (*22*). However, the orders of the reaction for oxygen and methanol did not necessarily coincide. According to the reaction mechanism proposed, oxidation of methanol takes place in the following manner,

$$CH_3OH + (O) \xrightarrow{k_1} HCHO + H_2O + (\ )$$

$$(\ ) + \tfrac{1}{2} O_2 \xrightarrow{k_2} (O)$$

where (O) and ( ) denote active site and reduced site, respectively. On the basis of this reaction scheme, kinetic equations are given relating to the coverage of active site (θ) and the rate of methanol oxidation (r) in the following.

$$\frac{1}{\theta} = 1 + \frac{k_1 P_m}{k_2 P_0^{1/2}} \qquad (3)$$

$$\frac{1}{r} = \frac{1}{k_1 P_m} + \frac{1}{k_2 P_0^{1/2}}. \qquad (4)$$

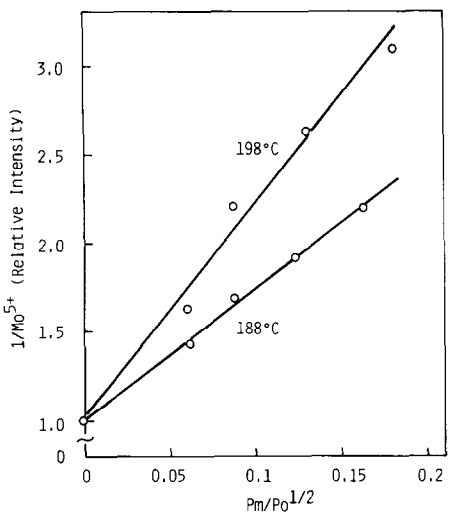

FIG. 6. Plots of $1/Mo^{5+}$ against $P_m/P_0^{1/2}$, in which P_0 was varied with a constant P_m (0.0382 atm).

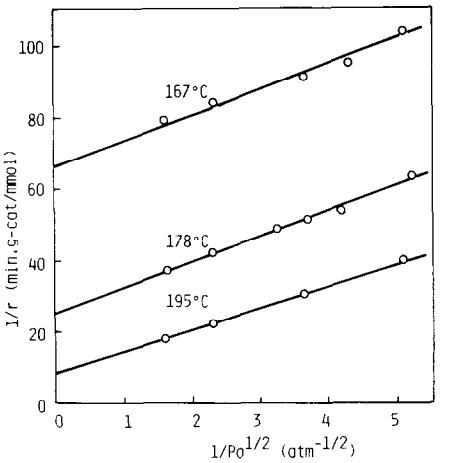

FIG. 7. Plots of $1/r$ against $1/P_0^{1/2}$.

The findings above suggest that the oxidized active sites may be ascribed to the Mo^{5+} rather than the Mo^{6+}, and it follows that $1/\theta$ may be given as $1/[Mo^{5+}]$. Based on Eq. (3), therefore, plots of $1/[Mo^{5+}]$ against $P_m/P_0^{1/2}$ give a straight line with a slope of (k_1/k_2). On the other hand, values of k_1 and k_2 may be obtained by applying the rate of methanol oxidation in a differential reactor to Eq. (4). The rate constants k_1 and k_2, and their ratio were obtained and compared by both measurements.

The ESR spectrum of Mo^{5+} was measured by varying the partial pressure of oxygen against a constant partial pressure of methanol. As observed above, the signal intensity decreased with decreasing partial pressure of oxygen. Reciprocals of the resultant signal intensities were plotted against $P_m/P_0^{1/2}$ from Eq. (3) and are shown in Fig. 6. These exhibited straight lines with an intercept of 1, as expected from Eq. (3). The ratios (k_1/k_2) at 188 and 198°C were calculated from these slopes. On the other hand, plots of $1/r$ against $1/P_0^{1/2}$, reproduced in Fig. 7, gave k_1 and k_2 from the intercept and the slope, respectively. Furthermore, k_1 and k_2 were also obtained from the plots in Fig. 8, in which the rate of methanol oxidation was measured by varying the par-

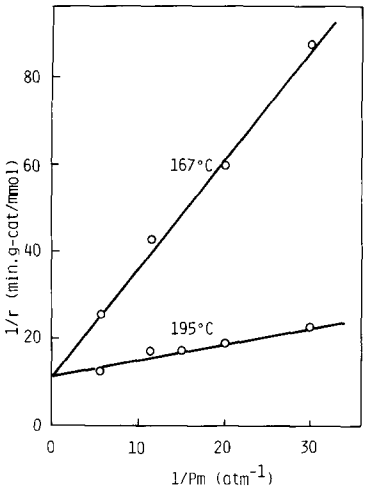

FIG. 8. Plots of $1/r$ against $1/P_m$.

tial pressure of methanol. The rate constants obtained from the data shown in Figs. 7 and 8 agreed well within the experimental error. Consequently, kinetic Eq. (4) derived from the proposed oxidation–reduction mechanism seems to be confirmed.

The (k_1/k_2) ratios obtained from the SnO_2–MoO_3 system are summarized in Fig. 9 by showing log (k_1/k_2) against the reciprocal absolute temperature. The values are shown in a simple relationship irrespective of measurement methods. It is therefore confirmed that the oxidation of methanol over the SnO_2–MoO_3 catalyst proceeds via the Mo^{5+} in the oxidation–reduction mechanism.

Measurements with Other Catalysts and Reactants

Methanol oxidation over TiO_2–MoO_3 proceeded selectively at higher conversion levels than over Fe_2O_3–MoO_3, as far as our experiments were concerned. MoO_3–SiO_2, however, possessed only a slightly higher activity than unsupported MoO_3. In ESR *in situ* measurements, the number of Mo^{5+} on TiO_2–MoO_3 (g = 1.90) and MoO_3–SiO_2 (g = 1.96) decreased with decreasing partial pressure of oxygen, as was found over SnO_2–MoO_3. Plots of $1/[Mo^{5+}]$ against $P_m/P_O^{1/2}$ showed straight lines with an intercept of 1, and these plots made it possible to calculate the ratio (k_1/k_2). The kinetic expression given in Eq. (4) was valid also for these catalysts, and rate constants were obtained from kinetic measurements. Comparison of the (k_1/k_2) values for the TiO_2–MoO_3 and MoO_3–SiO_2 systems in Fig. 9 indicates the consistency between the ESR and kinetic measurements. The conclusions above regarding SnO_2–MoO_3 are therefore approximately applied also to methanol oxidation over TiO_2–MoO_3 and MoO_3–SiO_2.

The behavior of the Mo^{5+} on SnO_2–MoO_3 during reaction was then investigated with C_2H_5OH, 2-C_3H_7OH, and C_3H_6 as reducing agents. The number of Mo^{5+} on SnO_2–MoO_3 decreased with increasing partial pressure of C_2H_5OH or 2-C_3H_7OH, and the calculated values of (k_1/k_2) at 162°C were 34.4 and 10.8 for ethanol and 2-propanol, respectively, both much greater than found for methanol (1.5).

Figure 10 shows the variation in relative intensity of Mo^{5+} signal on SnO_2–MoO_3 and MoO_3–SiO_2 during oxidation of propylene. Under reducing atmosphere, the signal intensity decreased on SnO_2–MoO_3, while it

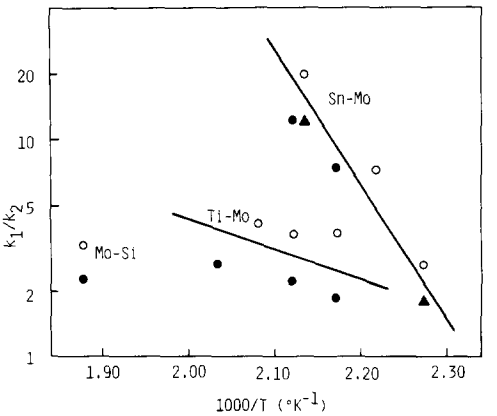

FIG. 9. Comparison of the ratios (k_1/k_2) from ESR (○) and kinetic (●, ▲) measurements over SnO_2–MoO_3, TiO_2–MoO_3, and MoO_3–SiO_2. The kinetic measurements were performed when either P_O(●) or P_m (▲) was varied.

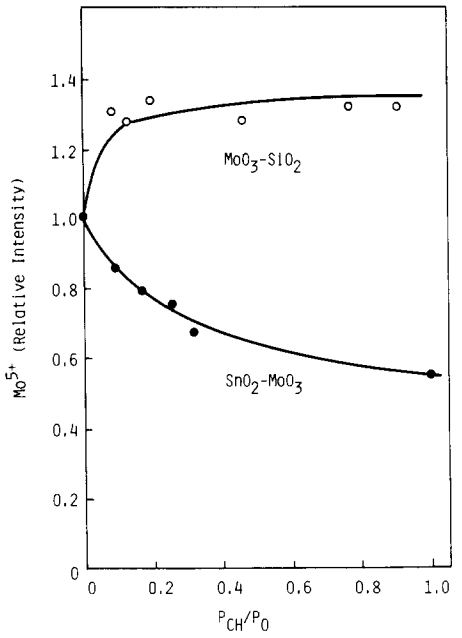

FIG. 10. Variation in relative intensity of Mo^{5+} with P_{CH} (partial pressure of propylene)/P_O on MoO_3–SiO_2 and SiO_2–MoO_3 at 278°C.

increased rapidly to become steady state on MoO_3–SiO_2. It was found that the Mo^{5+} on SnO_2–MoO_3 is not only reduced by alcohols but also by propylene in the oxidation reaction.

DISCUSSION

The mixed SnO_2–MoO_3 catalyst has been known for its peculiar activity in the oxidation of propylene (*19, 23*) and ethylbenzene (*20*). Catalytic activities are much enhanced by mixing these oxides, as described in this communication. However, detailed investigations of the structure of the mixed oxide did not detect a new compound consisting of SnO_2 and MoO_3 (*19, 20*), and it was believed that active sites could be attributed essentially to the boundary surface of SnO_2 and MoO_3.

In addition, the concentration of Mo^{5+} was increased by mixing SnO_2 with MoO_3. This Mo^{5+} was very stable and was not oxidized to Mo^{6+} even by calcination at 500°C, and fresh samples possessed Mo^{5+} to nearly the same degree as the aged one. It seems therefore that the Mo^{5+} is stabilized by neighboring SnO_2, and is concentrated at the boundary surface. In other words, the Mo^{5+} on SnO_2–MoO_3 can be regarded as a relatively unoxidizable species under these conditions. Stabilization of the Mo^{5+} through neighboring Mo–O–Al bonding has been discussed previously by Giordano *et al.* (*24*) in the case of MoO_3/Al_2O_3. This characteristic Mo^{5+} on SnO_2–MoO_3 is quite different from that found for Mo^{5+} on Bi_2O_3–MoO_3, because the latter can interact with adsorbed oxygen at room temperature and disappears easily by oxidation at a high temperature (*13, 18*). One can expect that these binary oxide catalysts possess different states of the Mo^{5+}.

Furthermore, it has been reported by Takita, *et al.* (*25*) that the solid acidity increases on mixing SnO_2 and MoO_3. This increase in the acidity may be associated with the Mo^{5+}, as mentioned above. The origin of acidity may be appeared by the interaction of water and Mo^{5+}, as indicated by Giordano *et al.* (*26*), i.e.,

$$Mo^{5+} + H_2O \rightarrow (Mo^{5+}\text{–}OH)^- + H^+$$

Thus forming (Mo^{5+}–OH) species may have a rôle of activating methanol, as described below.

Comparison of the reduction rates for Mo^{5+} (ESR) and Mo^{6+} (ir and gravimetry) shows that the Mo^{5+} is highly reactive, and can be regarded as the active site for methanol oxidation on SnO_2–MoO_3. ESR *in situ* measurements also add support to this hypothesis, because the derived ratio of rate constants (k_1/k_2) was in good agreement with that determined from kinetic measurements. The high activity of the Mo^{5+} may also be found in other binary oxides such as TiO_2–MoO_3 for the oxidation of methanol, or in SnO_2–MoO_3 for the oxidation of ethanol and 2-propanol. However, the rate constants obtained by the kinetic measurements were about 10 times as much as those derived from the reduction–reoxidation cycle of Mo^{5+}, though these ratios

were fairly consistent (Table 1). This difference may originate from the uncertainty of the radical concentration of Mo^{5+}, N_t, or from delayed reaction due to the immersed bulk sites. Therefore, all of the Mo^{5+} may not be available as active oxidized sites while the reaction is in progress.

The oxidized Mo^{5+} site probably turns into Mo^{4+} or Mo^{3+} on reduction. It is not easy to decide at present which is plausible reduced state of molybdenum ion. If the reduced site is the Mo^{4+}, which can be usually observed in reduced molybdenum oxide, and if the oxidized surface may be represented as in Fig. 11 (*24*), the reaction mechanism can be described as follows. Methanol may initially interact with Mo^{5+}–OH to give a surface methoxy group in place of an OH-group. This is followed by abstraction of the hydrogen to produce formaldehyde. This is repeated after reoxidation of the surface with oxygen.

It is well known that methanol yields methoxy radicals under electron-bombardment, and the OH group exchanges easily with D_2O to produce CH_3OD in a liquid state. Also in discussing the reaction route for methanol oxidation, the methoxy group attached to the metal cation has been regarded as one of the most likely species (*4, 7*). However, it seems that the rate-determining step involves the cleavage of the C–H bond. Iwasawa *et al.* (*27*) has also discussed the reaction mechanism of oxidation of ethanol on an Mo-fixed catalyst, and

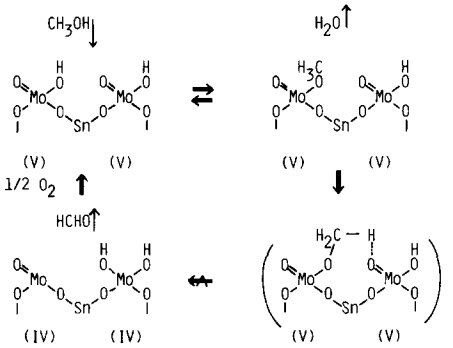

FIG. 11. Reaction mechanism of methanol oxidation on SnO_2–MoO_3 catalyst.

regarded the abstraction of a hydrogen of methyl group as the rate-determining step. Evmenenko and Gorokhobatskii (*8*) indicated that the high reactivity of ethyl alcohol was due to a smaller bond energy of RC(OH)–H in ethanol (88 kcal/mol) than in methanol (92 kcal/mol). Therefore, the reaction most likely proceeds via the methoxy ion, followed by abstraction of hydrogen in the slowest step. This scheme is not inconsistent with the result obtained by Pernicone *et al.* (*7, 22*) in which the addition of water to the reaction system suppressed the reaction rate.

Sancier *et al.* (*13*) have previously reported that the concentration of Mo^{5+} on Bi_2O_3–MoO_3 and on SiO_2-supported MoO_3 increased after the addition of propylene, and the electron transfer, $Mo^{6+} + e^- \rightarrow Mo^{5+}$, was associated with the adsorption of $C_3H_6^+$. Their result for the MoO_3–SiO_2–propylene system was confirmed in this paper (Fig. 10). Therefore, the findings on propylene oxidation by Sancier *et al.* are directly contrary to our results on methanol oxidation, because the concentration of Mo^{5+} decreased upon the reduction by CH_3OH. One can suggest therefore that oxidations of propylene and methanol occur primarily at different active sites, i.e., Mo^{6+} and Mo^{5+}, respectively. In fact, propylene oxidation is fast on Bi_2O_3–MoO_3 in which the concentration of Mo^{6+} was increased by mixing of Bi_2O_3 (*10, 13*), while methanol is readily oxidized on SnO_2–MoO_3 which had an enhanced concentration of Mo^{5+}. Availability of molybdenum sites with different oxidation states was reported by Giordano *et al.* (*28*).

ESR *in situ* measurement could not be applied to the Fe_2O_3–MoO_3 catalyst, because the broad signal due to the iron magnetic resonance obscures the Mo^{5+} field (*2*). It is suggested that one of the active phase for this reaction may be a spinel-type compound, $Fe_2(MoO_4)_3$. It may be also indicated that the MoO_3 component in Fe_2O_3–MoO_3 shares common features with the MoO_3 component in SnO_2–MoO_3, be-

cause the activity of formaldehyde formation in the Fe_2O_3–MoO_3 system is ascribed to MoO_3, and much heightened by mixing with Fe_2O_3.

ACKNOWLEDGMENTS

The authors wish to thank Dr. W. H. Quayle for helpful discussions.

REFERENCES

1. Adkins, H., and Peterson, W. R., *J. Amer. Chem. Soc.* **53**, 1512 (1931).
2. Boreskov, G. K., Kolovertnov, G. D., Kefeli, L. M., Plyasova, L. M. Karakchiv, L. G., and Mastikhin, V. N., *Kinet. Katal.* **7**, 144 (1966).
3. Pernicone, N., Liberti, G., and Ersini, L., *Proc. Int. Congress Catal. 4th* (Moscow, 1968) p. 287 (1968).
4. Novakova, J., Jiru, P., and Zavadil, V., *J. Catal.* **21**, 143 (1971).
5. Jiru, P., Wichterlova, B., and Tichy, T., *Proc. Int. Congr. Catal., 3rd Amsterdam* **1**, 199 (1965).
6. Mann, R. S., and Dosi, M. K., *J. Catal.* **28**, 282 (1973).
7. Pernicone, N., Lazzerin, F., Liberti, G., and Lanzavecchia, G., *J. Catal.* **14**, 293 (1969).
8. Evmenenko, N. P., and Gorokhobatskii, Ya. B., *Kinet. Katal.* **11**, 130 (1970).
9. Niwa, M., Mizutani, M., and Murakami, Y., *Nippon Kagaku Kai-shi* **1977**, 757.
10. Peacock, J. M., Sharp, M. J., Parker, A. J., Ashmore, F. G., and Hockey, J. A., *J. Catal.* **15**, 379 (1969).
11. Seshadri, K. S., and Petrakis, L., *J. Phys. Chem.* **74**, 4102 (1970).
12. Seshadri, K. S., Massoth, F. E., and Petrakis, L., *J. Catal.* **19**, 95 (1970).
13. Sancier, K. M., Dozono, T., and Wise, H., *J. Catal.* **23**, 270 (1971).
14. Burlamacchi, L., Martini, G., and Ferroni, E., *JCS Faraday Trans. I* **68**, 1586 (1972).
15. Akimoto, M., and Echigoya, E., *J. Catal.* **29**, 191 (1973).
16. Niwa, M., Hattori, T., Takahashi, M., Shirai, K., Watanabe, M., and Murakami, Y., *Anal. Chem.* **51**, 46 (1979).
17. Mann, R. S., and Hahn, K. W., *Anal. Chem.* **39**, 1315 (1967).
18. Sancier, K. M., Wentrcek, P. R., and Wise, H., *J. Catal.* **39**, 141 (1975).
19. Buiten, J., *J. Catal.* **10**, 188 (1968).
20. Araki, M., Nishimura, I., Hayakawa, T., Takehira, K., and Ishikawa, T., *Shokubai* **14**, 47 (1972).
21. Mann, R. S., and Hahn, K. W., *J. Catal.* **15**, 329 (1969).
22. Pernicone, N., Lazzerin, F., and Lanzavecchia, G., *J. Catal.* **10**, 83 (1968).
23. Tan, S., Moro-oka, Y., and Ozaki, A., *J. Catal.* **17**, 132 (1970).
24. Giordano, N., Bart, J. C. J., Castellan, A., and Vaghi, A., Climax First Int. Conf. Mo., 194 (1974).
25. Takita, Y., Ozaki, A., and Moro-oka, Y., *J. Catal.* **27**, 185 (1972).
26. Giordano, N., Vaghi, A., Bart, J. C. J., and Castellan, A., *J. Catal* **38**, 11 (1975).
27. Iwasawa, Y., Nakano, Y., and Ogasawara, S., *JCS Faraday Trans. I* **12**, 2968 (1978).
28. Giordano, N., Meazza, M., Castellan, A., Bart, J. C. J., and Ragaini, V., *J. Catal.* **50**, 342 (1977).
29. Trifiro, F., Notarbartolo, S., and Pasquon, I., *J. Catal.* **22**, 324 (1971).
30. Novakova, J., Jiru, P., and Zavadil., V., *J. Catal.* **17**, 93 (1970).